

Journal of  
**Applied Remote Sensing**

**Development of a widely tunable  
amplified diode laser differential  
absorption lidar for profiling  
atmospheric water vapor**

Michael D. Obland  
Kevin S. Repasky  
Amin R. Nehrir  
John L. Carlsten  
Joseph A. Shaw



# Development of a widely tunable amplified diode laser differential absorption lidar for profiling atmospheric water vapor

Michael D. Obland,<sup>a,b</sup> Kevin S. Repasky,<sup>c</sup> Amin R. Nehrir,<sup>c</sup> John L. Carlsten,<sup>a</sup> and Joseph A. Shaw<sup>c</sup>

<sup>a</sup> Montana State University, Physics Department, EPS 264, Bozeman, MT 59717, USA  
carlsten@physics.montana.edu

<sup>b</sup> NASA Langley Research Center, 100 NASA Road, M/S 420, Hampton, VA, 23681, USA  
Michael.D.Obland@NASA.gov

<sup>c</sup> Montana State University, Electrical and Computer Engineering Department, Cobligh 610, Bozeman, MT 59717, USA  
repasky@ece.montana.edu

**Abstract.** This work describes the design and testing of a highly-tunable differential absorption lidar (DIAL) instrument utilizing an all-semiconductor transmitter. This new DIAL instrument transmitter has a highly-tunable external cavity diode laser (ECDL) as a seed laser source for two cascaded commercial tapered amplifiers. The transmitter has the capability of tuning over a range of  $\sim 17$  nm centered at about 832 nm to selectively probe several water vapor absorption lines. This capability has been requested in other recent DIAL experiments for wavelengths near 830 nm. The transmitter produces pulse energies of approximately 0.25  $\mu$ J at a repetition rate of 20 kHz. The linewidth is exceptionally narrow at  $<0.3$  MHz, with frequency stability that has been shown to be  $\pm 88$  MHz and spectral purity of 0.995. Tests of the DIAL instrument to prove the validity of its measurements were undertaken. Preliminary water vapor profiles, taken in Bozeman, Montana, agree to within 5-60% with profiles derived from co-located radiosondes 800 meters above ground altitude. Below 800 meters, the measurements are biased low due to a number of systematic issues that are discussed. The long averaging times required by low-power systems have been shown to lead to biases in data, and indeed, our results showed strong disagreements on nights when the atmosphere was changing rapidly, such as on windy nights or when a storm system was entering the area. Improvements to the system to correct the major systematic biases are described.

**Keywords:** lidar, absorption, semiconductor lasers, tunable lasers, remote sensing.

## 1 INTRODUCTION

Water vapor in the lower troposphere plays a critical role in both weather and climate and detailed knowledge of its concentration profiles and fluxes is needed for forecasts and model predictions. Water vapor is primarily contained within the lowest 3 km of the troposphere with a high spatial and temporal flux [1-3]. Radiosondes are currently used to obtain routine water vapor profiles, but this technique can only provide information at one location at one point in time and cannot easily be used to monitor the spatial and temporal changes of the water vapor concentrations [3]. A need exists for remote sensing tools capable of monitoring tropospheric water vapor profiles continuously in time at many locations [4].

Significant progress has been demonstrated in developing and using high-performance lidars for profiling atmospheric water vapor at isolated research sites and in detailed process studies, from both the ground [3, 5-12] and the air [13-20]. However, more routine deployment of lidars for water vapor profiling at multiple sites will require smaller, mostly

autonomous, lower-cost systems that are eye-safe. The trend in recent years toward smaller and more robust lidar systems has resulted in a significant increase in the use of lidars for aerosol and cloud studies [21-25] and a similar trend is beginning to emerge for water vapor lidars. For example, previously large and complex Raman lidar systems are now being packaged in moderately sized trailers and operated routinely in long-term, largely unattended field deployments [3, 6, 12]. However, even smaller Raman lidars require high-power pulsed lasers because the Raman scattering cross section is  $\sim 4$  orders of magnitude below that of both Rayleigh and Mie backscatter [26,27]. Raman lidar systems also require external calibration.

Differential absorption lidar (DIAL) [7, 26-28] systems also are moving toward smaller size and lower-cost, which may someday allow deployment in unattended networks [5, 29-34]. DIAL measurements require measuring backscattered light at wavelengths on and off an absorption line, with wavelengths sufficiently close to each other that aerosol scattering and other systematic features of the measurement cancel in a ratio. The ratio of the on- and off-line measurements can be used to determine a vertical profile of the constituent concentration. Current systems have largely used solid state lasers, dye lasers, and optical parametric oscillators as their transmitters, but these systems are not as small as what can be achieved with diode lasers.

One promising avenue of research toward compact water vapor DIAL instruments is to use semiconductor laser transmitters [5, 29-35]. Diode lasers are compact, inexpensive, can be tuned readily, and have good spectral coverage in the near infrared spectral region where appropriate water vapor absorption lines exist. In the early 1990s, the increased availability of high-power diode lasers and photon-counting avalanche photodiode detectors led to the proposal of diode DIAL systems for boundary layer water vapor profiling [5, 29,30]. However, remaining challenges included low laser power and hence low signal return, spectrally broad laser pulses, and insufficiently precise or stable laser tuning.

Several variations on the theme of diode laser transmitters with avalanche photodiode (APD) detectors in photon-counting mode have been studied numerically [29, 30, 33, 35], but few systems have been implemented. Rall [5] built a DIAL system using an externally modulated AlGaAs laser near 811.6 nm and achieved mean water vapor number density measurements that agreed with measured humidity values to within 6.5% and 20% in integrated path ( $\sim 5$  km horizontal one-way path) and range-resolved (4 km horizontal one-way path) modes, respectively. Oh et al. [35] reported initial experimental results from a diode-pumped Cr:LiSAF laser operating near 824.6 nm with an APD detector. They showed on- and off-line water vapor absorption profiles from the ground up to approximately 3 km, but the long time delay ( $\sim 1$  hour) between measurements prevented the retrieval of a DIAL profile. Prasad et al. [31] describe a Cr:LiSAF laser for DIAL operation on a Unpiloted Airborne Vehicle (UAV), and show measurements from a breadboard system that have loose agreement with a regional radiosonde profile up to approximately 1.4 km.

Little and Papen [32] reported nighttime data with multi-hour averaging times from a fiber-based lidar, showing reasonable agreement between their data, simulations, and a regional radiosonde profile up to an altitude of 2 km. More recently, Machol et al. [34] reported initial water vapor DIAL measurements from a system based on a distributed feedback (DFB) diode laser used as a seed for a diode flared amplifier, operating at 823 nm with 0.8 nm of tuning. This system provides 0.15  $\mu\text{J}$  pulse energy at pulse repetition frequencies of 6-10 kHz. Their horizontal-path measurements showed good agreement between the DIAL retrieval and surface *in situ* sensor water vapor data; they also showed zenith measurements that agreed well with a radiosonde profile between 800 and approximately 2500 m altitude. Machol et al. [34] note that new laser transmitter designs are needed for better spectral coverage and larger tuning ranges, calling for "a new laser [with] a tuning range that accesses a larger selection of good water-vapor lines...". They also note that

their DFB laser is no longer available from the vendor, making it particularly important to have alternate laser transmitter sources.

The design and demonstration of a DIAL laser transmitter based on a tunable external cavity diode laser [36-38] (ECDL) is presented in this paper as a possible alternate seed laser source. The laser source development group at Montana State University (MSU) has extensive experience building high-quality ECDL's, which was leveraged to develop the highly tunable transmitter for the water vapor DIAL. The ECDL uses spectrally filtered optical feedback from a Littman-Metcalf external cavity to produce a tuning range from 824 nm to 841 nm. This 17 nm tuning range allows the laser transmitter to access many water vapor absorption lines with varying absorption strengths. The output from the ECDL was used to seed two cascaded, commercially available tapered amplifiers (TA) to produce an amplified cw output of up to 500 mW peak power. Pulsed operation of the laser transmitter was achieved by modulating the cw output with an acousto-optic modulator (AOM). As an initial demonstration of its wide tuning capability, the laser transmitter was used to make horizontal path-integrated water vapor measurements for open-air path lengths from 0.35 km to 1.71 km, at both 829.022 nm and 831.615 nm wavelengths. These horizontal-path measurements were made with the aid of hard-target reflection, to focus on testing the tuning capability of the transmitter. The data set is compared with theoretical calculations based on the HiTRAN-PC line-by-line radiative transfer software [39]. The laser transmitter was then used to make preliminary vertical measurements as an initial step toward the intended atmospheric water vapor profiling system. These vertical measurements were compared to data from a co-located radiosonde and the biases found and subsequent necessary corrections to the system are described herein.

This paper is organized as follows. Section 2 discusses water vapor absorption line selection. Section 3 describes the system design and layout. System characterization and testing are explained in Sec. 4 and subsequent initial measurements are discussed in Sec. 5. Finally, concluding remarks are included in Sec. 6.

## 2 WATER VAPOR ABSORPTION LINE SELECTION

The theory, development, and nuances of the lidar and DIAL equations have been described extensively in the literature and will not be repeated here [7, 40]. DIAL measurements require signal retrievals at two wavelengths,  $\lambda_{\text{on}}$ , located on the line center of an absorption line of some atmospheric constituent such as ozone or water vapor, and  $\lambda_{\text{off}}$ , located some spectral distance away from the absorption line center, in another part of the absorption continuum for the case of ozone or completely clear of the absorption line in the case of water vapor [40]. Therefore, particularly for water vapor DIAL measurements, selection of the wavelengths  $\lambda_{\text{on}}$  and  $\lambda_{\text{off}}$  is of critical importance to the accuracy of the measurement.

Three sources of error need to be considered when selecting these wavelengths. First, absorption line strengths, and therefore line shapes and absorption cross sections, of the water vapor line at  $\lambda_{\text{on}}$  can be strong functions of temperature, causing errors in the measurement due to the uncertainty in temperature as the transmit laser pulse propagates through the atmosphere. Second, the optical depth produced by the absorption line must be considered, as absorption lines can either be too strongly absorbing, resulting in too low of a return signal, or too weak, resulting in not enough difference between the on- and off-line return signals. Third, the presence of other absorption features near to the absorption line being used can cause errors to be made in the absorption cross section measurement of this line, unless these other features are properly accounted for. Therefore,  $\lambda_{\text{on}}$  and  $\lambda_{\text{off}}$  should be clear of nearby absorption features. A balance must be struck between these three criteria of temperature sensitivity, optical depth, and nearby absorption features when finding an appropriate water vapor absorption line for DIAL measurements.

Our procedure for selecting a water vapor absorption line closely followed the methods of Browell et al., 1991 [41]. Temperature sensitivity analysis involves calculating the error in the absorption cross section with temperature,  $d\sigma/dT$  [ $\text{cm}^2/\text{K}$ ], where  $\sigma = KV$  [ $\text{cm}^2$ ], across a range of temperatures, pressures, and ground-state transitional energies,  $E''$  [ $\text{cm}^{-1}$ ].  $K$  here is a function of the Doppler linewidth and absorption line strength.  $V$  is the Voigt profile, which is a convolution of the Lorentz and Gaussian profiles, and must be used in regions where both pressure and Doppler broadening effects are important. Using a Voigt profile is especially important at high altitude locations, such as Bozeman, Montana, where the ground level air pressure is already less than 1013.25 hPa. The goal of the analysis is to compute the range of  $E''$  values where  $d\sigma/dT$  is minimized, meaning errors due to temperature variations will be small. We first performed our temperature sensitivity analysis in the same region as Ref. 41, near 720 nm, to confirm that we could reproduce their results. We then applied a similar analysis to absorption lines in the 824 - 841 nm region. We also confirmed our results with Ambrico et al., 2000, who more recently showed results for temperature sensitivity analysis in much of the near infrared for a greater number of molecules than just water vapor [42]. Our results were nearly identical in both cases, and showed that the optimal  $E''$  limits for number density measurements that give error values of  $\pm 0.10\%$ /K between 200 K and 300 K for pressures changing from 1013.25 hPa to 253.3125 hPa are about 125-225  $\text{cm}^{-1}$ . Note that these values apply to number density measurements only; the optimal  $E''$  values for mixing ratio measurements will be different due to the mixing ratio having a different functional dependence on temperature.

After temperature sensitivity, the next limiting factor in the absorption line selection procedure is the strength of the line, or more specifically, the optical depth it produces. Optical depth (OD),  $\tau$  [unitless], is defined as  $\tau = \int_0^R N\sigma dr$ , where  $R$  [m] is the range of the measurement and  $N$  [ $\text{molecules}/\text{cm}^3$ ] is the number density of water vapor molecules. If the absorption line is too strong,  $\sigma$  will be relatively large compared to the off-line absorption, causing  $\tau$  to be too large and the on-line return signal to be too weak, since the signal goes as  $\exp(-\tau)$ . Conversely, if the absorption line is too weakly absorbing,  $\sigma$  will be relatively small compared to the off-line absorption, causing  $\tau$  to be too small and the on-line return signal to be undifferentiable from the off-line signal return. Differential absorption lidar error analysis has shown that the optimal value for  $\tau$  is  $<2$  up to the desired maximum range with a value for the differential OD within a layer in the range  $0.02 < \Delta\tau < 0.1$  in order to minimize errors while maximizing signal [43-45].

Because the optical depth is a function of the number density of water vapor molecules, the optimal strength absorption line will be dependent on the geographic location of the measurement. Water vapor lines that are suitable for Bozeman, Montana, a relatively dry climate, would be unusable in a highly humid tropical region, for example. Some *a priori* knowledge of the behavior of water vapor in the region of interest is required. For our analysis, we analyzed archived temperature, pressure, and relative humidity data collected by the Optical Remote Sensor Laboratory's weather station located on the roof of Cobleigh Hall on the Montana State University campus from August 2005 through July 2006 [46] to produce an estimate of seasonal variation in water vapor number density. This weather station was located within a few meters of the eventual location of our DIAL instrument.

Figure 1 shows a plot of the horizontal path transmission calculated using HiTRAN-PC, a atmospheric-modeling software code [39], through a 1 km path length at standard temperature and pressure as a function of wavelength between 12195.1220  $\text{cm}^{-1}$  and 11848.3412  $\text{cm}^{-1}$  (820 nm and 844 nm), which includes the tuning range of the ECDL/TA transmitter system. All of the absorption features are due to water vapor. The water vapor lines in this region with optimal  $E''$  values for temperature sensitivity between 125 and 225  $\text{cm}^{-1}$  are listed in Table 1 with their corresponding line strengths, ground-state transitional energies, and full-widths at

half-maximum amplitude (FWHM). The transmission for a 1 km horizontal path using the US Standard Atmosphere model is also given to illustrate line strength differences.

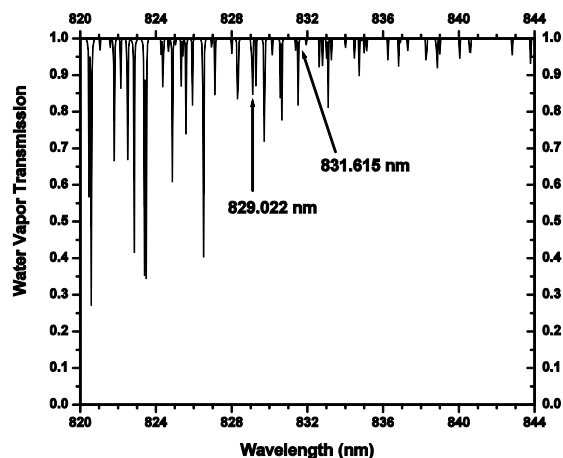


Fig. 1. A plot of the horizontal path transmission calculated using HiTRAN-PC through a 1 km path length as a function of wavelength accessible by the DIAL transmitter. The absorption features are due to water vapor.

Using the OD criteria and desired laser operating wavelength for our system to further limit the optimal absorption lines left the nine absorption lines listed in bold italics in Table 1. Rough limits of the average water vapor mass density that produces reasonable optical depth values across a 2 km vertical path in the Bozeman, MT, atmosphere are listed for reference. Again, it must be emphasized that the optimal water vapor absorption line chosen for any individual system will depend on the laser parameters of that system, such as the wavelengths available to the laser and the ability of the laser to tune away from absorption features near the on-line wavelength, and the environmental conditions in which it operates. Weaker absorption lines will be useful in more humid environments than Bozeman, and stronger absorption lines will be useful in dryer climates.

The final criterion for selecting a suitable water vapor absorption line is to ensure that the absorption line is adequately isolated from other absorption features of water vapor or other gasses. Figure 2 produced by HiTRAN-PC, using the HiTRAN database [39], shows the absorption features due to water vapor in the  $12059.8167 - 12086.0527 \text{ cm}^{-1}$  (829.2 - 827.4 nm) range and their relative wavelength spacing.

The water vapor absorption line at  $12074.5689 \text{ cm}^{-1}$  (828.187 nm, vacuum wavelength) was ultimately selected for use in the MSU water vapor DIAL. It meets the temperature sensitivity requirements, has a line strength that gives nearly optimal optical depth during most months of the year in Bozeman, Montana, and is sufficiently isolated from other nearby absorption features. The off-line vacuum wavelength was chosen to be  $12073.1099 \text{ cm}^{-1}$  (828.287 nm) to minimize interference with other absorption features, in particular the absorption line located at  $12075.8654 \text{ cm}^{-1}$  (828.098 nm). The final on-line and off-line wavelengths are indicated in Fig. 2.

Table 1. Candidate water vapor absorption lines between 12195.1220  $\text{cm}^{-1}$  and 11848.3412  $\text{cm}^{-1}$  (820 nm and 844 nm). The water vapor lines listed have  $E''$  values between 125 and 225  $\text{cm}^{-1}$ . The transmission values (column 6) were calculated using HiTRAN for a 1 km horizontal path with standard atmospheric conditions. The average absolute humidity (AH, water vapor mass density) in a 2 km vertical path that will yield reasonable optical depth values in the Bozeman, MT, atmosphere are listed in column 7 for absorption line candidates for the system in this study.

| $\lambda$<br>(nm) | Wavenumber<br>( $\text{cm}^{-1}$ ) | FWHM<br>( $\text{cm}^{-1}$ ) | S<br>( $\text{cm}^{-1}/(\text{mol cm}^{-2})$ ) | $E''$<br>( $\text{cm}^{-1}$ ) | Trans.<br>(%) | AH<br>( $\text{g/m}^{-3}$ ) |
|-------------------|------------------------------------|------------------------------|--|-------------------------------|---------------|-----------------------------|
| 839.72            | 11908.73148                        | 0.1727                       | 2.96E-25                                       | 222.1                         | 97.929        |                             |
| 839.632           | 11909.97961                        | 0.1678                       | 9.14E-25                                       | 224.8                         | 93.555        |                             |
| 839.137           | 11917.00521                        | 0.1894                       | 9.00E-26                                       | 136.8                         | 99.42         |                             |
| 839.007           | 11918.85169                        | 0.1938                       | 5.95E-25                                       | 134.9                         | 96.317        |                             |
| 838.73            | 11922.78802                        | 0.1883                       | 1.98E-25                                       | 136.2                         | 98.724        |                             |
| 838.647           | 11923.96801                        | 0.1905                       | 9.35E-25                                       | 173.4                         | 94.175        |                             |
| 837.555           | 11939.51442                        | 0.1889                       | 2.87E-25                                       | 206.3                         | 98.159        |                             |
| 836.966           | 11947.91664                        | 0.1882                       | 7.28E-25                                       | 212.2                         | 95.377        |                             |
| 832.859           | 12006.83429                        | 0.1894                       | 7.49E-25                                       | 212.2                         | 95.28         |                             |
| 831.518           | 12026.19787                        | 0.201                        | 1.25E-25                                       | 206.3                         | 99.244        |                             |
| 830.73            | 12037.60548                        | 0.2062                       | 1.10E-25                                       | 136.2                         | 99.35         |                             |
| 830.546           | 12040.2723                         | 0.205                        | 1.04E-25                                       | 136.2                         | 99.384        |                             |
| 830.223           | 12044.9566                         | 0.1979                       | 1.90E-25                                       | 224.8                         | 98.832        |                             |
| 830.103           | 12046.69782                        | 0.2096                       | 1.36E-25                                       | 134.9                         | 99.211        |                             |
| 829.659           | 12053.14473                        | 0.1857                       | 8.70E-25                                       | 222.1                         | 94.433        |                             |
| <b>829.18</b>     | <b>12060.10758</b>                 | <b>0.2011</b>                | <b>1.04E-23</b>                                | <b>222.1</b>                  | <b>53.127</b> | <b>3-10</b>                 |
| <b>829.022</b>    | <b>12062.40606</b>                 | <b>0.1951</b>                | <b>3.02E-23</b>                                | <b>224.8</b>                  | <b>15.043</b> | <b>&lt;3</b>                |
| <b>828.429</b>    | <b>12071.04049</b>                 | <b>0.1887</b>                | <b>2.75E-23</b>                                | <b>173.4</b>                  | <b>16.815</b> | <b>&lt;3</b>                |
| <b>828.187</b>    | <b>12074.5677</b>                  | <b>0.1962</b>                | <b>1.48E-23</b>                                | <b>212.2</b>                  | <b>39.824</b> | <b>&lt;7</b>                |
| 828.098           | 12075.86542                        | 0.1894                       | 6.18E-25                                       | 206.3                         | 96.085        |                             |
| <b>827.896</b>    | <b>12078.81183</b>                 | <b>0.2035</b>                | <b>8.07E-24</b>                                | <b>136.8</b>                  | <b>61.507</b> | <b>4-10</b>                 |
| <b>827.879</b>    | <b>12079.05986</b>                 | <b>0.1894</b>                | <b>4.86E-24</b>                                | <b>206.3</b>                  | <b>73.073</b> | <b>7-10</b>                 |
| 827.768           | 12080.67961                        | 0.2056                       | 1.00E-25                                       | 134.9                         | 99.407        |                             |
| <b>827.662</b>    | <b>12082.2268</b>                  | <b>0.2116</b>                | <b>2.76E-23</b>                                | <b>136.8</b>                  | <b>20.269</b> | <b>&lt;4</b>                |
| 827.535           | 12084.08104                        | 0.2062                       | 1.07E-24                                       | 134.9                         | 93.84         |                             |
| <b>827.431</b>    | <b>12085.59989</b>                 | <b>0.202</b>                 | <b>1.04E-23</b>                                | <b>142.3</b>                  | <b>53.153</b> | <b>4-10</b>                 |
| 826.722           | 12095.96454                        | 0.2007                       | 3.76E-25                                       | 212.2                         | 97.734        |                             |
| 826.691           | 12096.41813                        | 0.2095                       | 1.72E-25                                       | 173.4                         | 99.003        |                             |
| <b>825.499</b>    | <b>12113.88506</b>                 | <b>0.2098</b>                | <b>6.48E-24</b>                                | <b>173.4</b>                  | <b>68.539</b> | <b>7-10</b>                 |
| 823.616           | 12141.58054                        | 0.1905                       | 1.71E-23                                       | 212.2                         | 32.304        |                             |
| 823.099           | 12149.20684                        | 0.1891                       | 1.29E-23                                       | 136.2                         | 43.298        |                             |
| 823.047           | 12149.97442                        | 0.1894                       | 1.30E-25                                       | 136.8                         | 99.164        |                             |
| 822.998           | 12150.69781                        | 0.1894                       | 2.84E-25                                       | 212.2                         | 98.185        |                             |
| 822.922           | 12151.81998                        | 0.1872                       | 3.90E-23                                       | 134.9                         | 7.809         |                             |
| 822.795           | 12153.69564                        | 0.1939                       | 5.90E-24                                       | 206.3                         | 68.915        |                             |
| 821.601           | 12171.35812                        | 0.2082                       | 1.95E-25                                       | 136.8                         | 98.864        |                             |
| 821.475           | 12173.22499                        | 0.1859                       | 1.74E-25                                       | 134.9                         | 98.862        |                             |
| 821.322           | 12175.49268                        | 0.1999                       | 1.17E-25                                       | 173.4                         | 99.285        |                             |
| 821.181           | 12177.58326                        | 0.2162                       | 2.44E-24                                       | 142.3                         | 87.131        |                             |
| 820.126           | 12193.24835                        | 0.1983                       | 4.04E-24                                       | 224.8                         | 77.93         |                             |
| 839.72            | 11908.73148                        | 0.1727                       | 2.96E-25                                       | 222.1                         | 97.929        |                             |

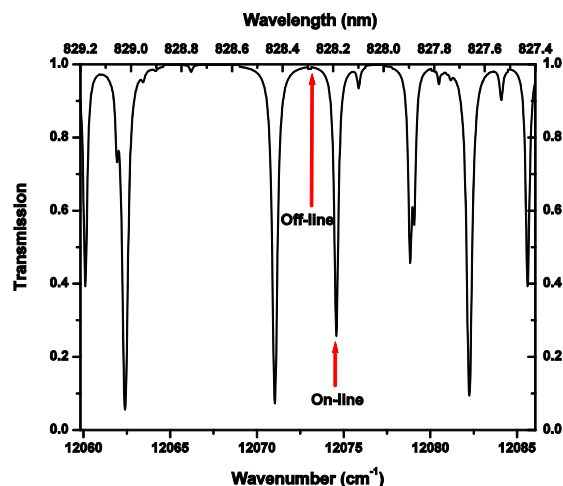


Fig. 2. A HiTRAN-PC plot at default values of 1013.25 hPa and 296 K across a 1.5 km horizontal path length, showing all absorption lines between  $12059.8167 \text{ cm}^{-1}$  and  $12086.0527 \text{ cm}^{-1}$  (829.2 - 827.4 nm). The final on- and off-line wavelengths selected for the water vapor DIAL are indicated.

### 3 SYSTEM DESIGN

The scattering cross section for the atmosphere, especially in a clear-air environment such as Bozeman where aerosols are relatively minimal, is very small and thus, careful attention had to be paid to the DIAL design to ensure that the maximum number of photons could be transmitted and then counted. The transmitter, receiver, and data acquisition subsystems are separately described in this section.

#### 3.1 Transmitter

The key to the entire water vapor DIAL described herein is the unique external cavity diode laser built at Montana State University that is being used as the seed laser for the DIAL transmitter. While diode lasers offer wide spectral coverage and tunability, especially in wavelength regions containing absorption features of scientifically interesting atmospheric constituents, they have not typically been used as the primary transmitter for DIAL instruments due to diodes typically possessing wide spectral bandwidths and low transmit powers. Certain external cavity configurations can narrow the spectral bandwidth and raise the spectral purity of the diode output, and optical amplifiers can be used to increase the transmit powers available in diode transmitters.

To address the diode's spectral bandwidth limitation, the MSU DIAL transmitter diode was placed in a Littman-Metcalf external cavity configuration [47] such that the output of the diode laser is incident on a diffraction grating, allowing for a stable tuning method to be employed. Another advantage of this configuration is that the output of the ECDL remains pointed in the same direction, unlike other configurations that steer the 0<sup>th</sup> order diffracted output beam, as in the Littrow configuration. A schematic of a ECDL in this configuration is shown in Fig. 3 with an accompanying picture in Fig. 4.

A 150-mW diode laser with a center wavelength of 830 nm (SDL-5421) is collimated using an aspheric lens with a focal length of 4.5 mm and a numerical aperture of 0.55 (Thor Labs 350230-B). The collimated light is next incident on a 1600 line/mm grating, 15 mm wide by 60 mm long by 10 mm thick (Spectrogon), at a grazing angle of 3 degrees, spatially

separating the wavelengths of the diode's broad spectral output. The zeroth-order reflection is used as the output for the ECDL. The first-order reflection from the diffraction grating is found from  $\cos \theta_{\text{out}} = \cos \theta_{\text{in}} - \lambda/d$  to be  $109^\circ$ , where  $\theta_{\text{in}}$  ( $\theta_{\text{out}}$ ) is the angle between the incoming (outgoing) beam and the plane of the diffraction grating,  $\lambda$  is the wavelength, and  $d$  is the line spacing of the diffraction grating. The first-order reflection is incident on a retro-reflecting roof prism that directs the light back into the diode laser via a second reflection from the diffraction grating, providing optical feedback to the diode laser and forcing the laser to run in a single longitudinal mode at the chosen wavelength. The advantage of using the prism over a mirror is that it is easier to align since it acts like a corner cube in the non-dispersive direction.

The spectral characteristics of the ECDL are defined by the frequency of the light fed back into the diode laser and the resonant condition that requires an integer number of half wavelengths to fit within the external cavity. Tuning the ECDL is accomplished by rotating the roof prism around a pivot point [48,49] to change the frequency of light fed back to the diode laser while simultaneously changing the external cavity length, so that a constant integer number of half wavelengths is maintained within the external cavity [37,38], allowing for continuous tuning. Fine rotation of the roof prism is achieved by applying a voltage to a piezo-electric stack (PZT, Thor Labs AE0505D16), giving mode-hop-free tuning of over 20 GHz at a fixed temperature. The roof prism can be rotated mechanically by a 3/16-100 screw for coarse tuning. The 3.8-cm-long external cavity has a free spectral range of 3.9 GHz.

The ECDL is placed on a thermo-electric cooler (TEC) for temperature stabilization, and monitored and controlled by a commercial temperature and current controller (ILX LDD3722) to within 0.1 degrees Celsius. The same controller is used to supply a drive current to the diode laser, which is operated in a continuous-wave (cw) mode. The output of the ECDL is sent through two Faraday isolators to prevent unwanted feedback from affecting its performance.

The ECDL performance is summarized as follows. The coarse tuning range varies from 824 nm to 841 nm by mechanically changing the angle of the retroreflective prism. By applying a DC voltage to the piezo-electric stack, we can also obtain a mode-hop-free tuning range greater than 20 GHz. The beginning and ending wavelengths of this tuning range can be altered by adjusting the diode temperature, typically between 19.2 and 20.2 degrees Celsius. The diode current is locked at about 37 mA. The full-width at half-maximum line-width is less than 200 kHz, as determined by beating experiments [50]. The maximum output power is 20 mW, with a side-mode suppression of greater than 45 dB, as measured on an optical spectrum analyzer (OSA). ECDLs have been built at Montana State University with similar performance at center wavelengths of 790, 808, 830, 850, 935, 1050, 1160, 1330, and 1540 nm. Other wavelengths such as 950 nm, where water vapor has strong absorption features, can be reached easily through simple modifications of the ECDL design. Commercial tunable ECDLs are also available [51]. The advantage of building them at Montana State University is that wavelengths specific to DIAL applications can be easily achieved. A detailed description of how the ECDL was designed and built can be found in Switzer, 1999 [52].

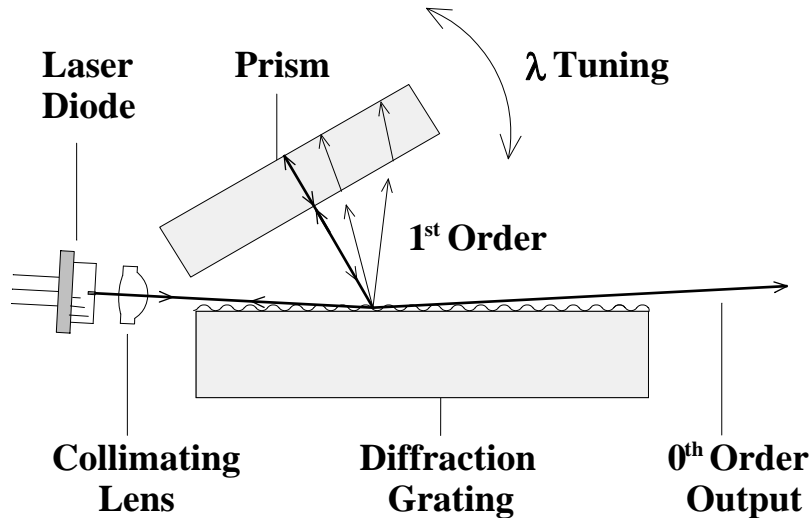


Fig. 3. A schematic of a tunable external cavity diode laser in a Littman-Metcalf configuration. The collimated light from a laser diode is incident on the diffraction grating. The zeroth order reflection is used as the output from the external cavity laser while the first order reflection is used to spatially separate the spectral output from the diode. The prism serves as a retroreflector to provide optical feedback to the diode laser via a second reflection from the diffraction grating and is used to control the operating frequency of the external cavity laser. Tuning is achieved by rotating the prism.

To address the ECDL's low output power limitation, which is set to  $< 20$  mW to extend the diode's lifetime and improve the tuning characteristics, the ECDL is used to injection seed a semiconductor tapered amplifier (Sacher Lasertechnik TA830) to obtain higher optical powers while maintaining the spectral properties of the seed laser. The seed power from the ECDL was only about 6 mW after traveling through two Faraday isolators to prevent optical feedback from damaging the diode, and therefore was too low to fully saturate the TA. In an attempt to increase the total transmit power above the  $\sim 120$  mW maximum power generated by the first TA, a second, cascaded tapered amplifier was added to the DIAL. The first TA can be used to seed and fully saturate the second TA, allowing it to operate at its maximum output power of  $\sim 450$  mW. Figure 5 shows how higher seed power makes an obvious difference in the output power of the second TA compared to the first. Even with low seed power, the spectral characteristics of the ECDL, including linewidth and tunability, are transferred to the output of the tapered amplifier [38]. Note that when the amplifier is not powered, about  $2 \mu\text{W}$  of power is still transmitted from the ECDL through the amplifier. Therefore, the ratio of the output of the amplifier when it is on to the transmitted power of the seed laser with the amplifier off is about 50 dB.

The amplifier's temperature and current are controlled and monitored by a commercial laser diode controller (Sacher Lasertechnik Pilot P3000). The first amplifier's temperature and current were set at about 21 degrees Celsius and 2.0 A. The output power of the first TA was kept to  $\sim 20$  mW for seeding the second TA, and therefore overheating was not a problem. Greater care had to be taken to adequately heat sink the second TA and hold its temperature stable at 21.0 degrees Celsius. The second TA was driven at a full current of  $\sim 2.8$  A. Figure 6 shows an OSA trace of the optical power at the amplifier output, plotted as a function of wavelength and attenuated to avoid damaging the OSA. A tuning range of 17 nm, from 824 to 841 nm, is obtained when the ECDL is tuned. The side-mode suppression ratio of the amplifier output reaches greater than 45 dB, which is identical to the ECDL output. For spatial quality,  $M^2$  values of the amplifier output beam have the typical values between 1.4

and 2.5, as claimed by the manufacturer. The wide tunability of this transmitter allows it to access any of the water vapor absorption lines in this region, shown in Fig. 1, giving it an unprecedented ability to choose the best absorption line for the given environmental conditions.

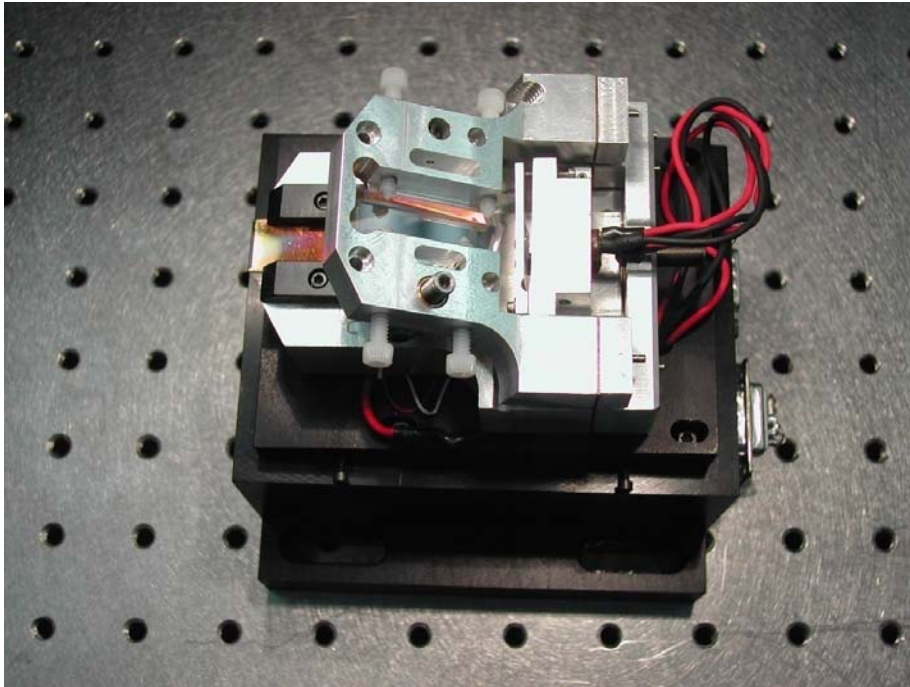


Fig. 4. A picture of an ECDL built at Montana State University. This laser can be tuned from 824 nm to 841 nm.

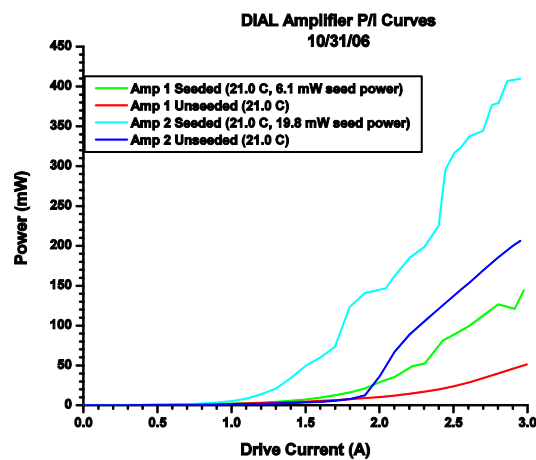


Fig. 5. Plots of output power versus drive current for the two amplifiers used in the DIAL experiment. Notice the large difference between amplifiers seeded, but not saturated, and seeded at nearly full seed power.

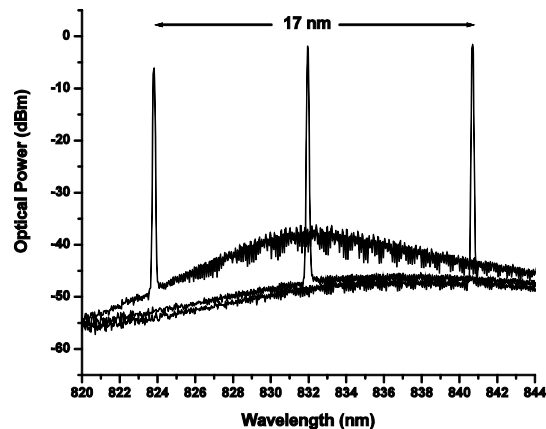


Fig. 6. A plot of the tunability of the DIAL laser transmitter, shown by three overlaid plots of the optical power of the injection seeded amplifier (attenuated to avoid damaging the OSA). The ECDL was tuned mechanically by adjusting the retroreflective prism to 824 nm (832 nm, 841 nm) and was used to seed the amplifier. The spectral output of the amplifier is controlled by the spectral properties of the injection seeded ECDL laser.

Two advantages to using these commercial tapered amplifiers are that they are easily available (although expensive) and work well at the necessary wavelength,  $\sim 830$  nm. The most important drawback is that pulsing them at the speeds necessary for DIAL measurements has so far proven unreliable. Several techniques were tried in an attempt to pulse the tapered amplifier. The TA itself has a pulsing option using external modulation, but the maximum rate that the amplifier could be cycled on and off was only 10 kHz, corresponding to a pulse length of 100  $\mu$ s (range resolution of 15 km), too long for the range resolutions required in the DIAL experiment. A cycling rate of at least 1 MHz was required to achieve pulse lengths of 1  $\mu$ s (range resolution of 150 meters) or less.

When pulsing the TA directly failed, we chose to use an acousto-optic modulator (AOM) made by Isomet (1205C-2). The advantages to using an AOM include that there is no frequency chirp in the transmitted beam and that each pulse is a near-perfect square shape in time. The drawback is that only about 66% of the light input to the AOM is transmitted through it into a pulsed beam, reducing the transmit power of an already low-power system.

Other studies have focused on DIAL systems with average powers of  $\sim 500$  mW or more [7, 45], which is far higher than the average power of  $\sim 5$  mW for this system. Some of the lack of output power can be compensated for with the use of higher laser repetition rates. Based on our calculations and experience with the system reported here and in subsequent experiments, the lowest average power limit that can produce useful meteorological profiles seems to be near the  $\sim 5$  mW of this system. Numerical simulations for very low-power DIAL systems need to be performed to calculate this lower limit.

### 3.2 Receiver

After scattering off of a molecule or particle in the atmosphere, the transmit photons were collected and focused by a 28-cm diameter commercial Schmidt-Cassegrain telescope (Celestron CGE1100) that uses a folded design, with a primary mirror at the bottom of the telescope housing that reflects light to a smaller secondary mirror located in the middle of the entrance aperture. The focused light was collimated for transmission through a narrowband interference filter (Barr Associates) centered at 828.01  $\pm$  0.05 nm in air. The bandpass of the

filter is shown in Fig. 7. The narrowband filter had a FWHM bandwidth of  $0.25 \pm 0.05$  nm and a peak transmission of  $> 50\%$ . From there, the photons were focused onto an optical fiber, which then carried them to an avalanche photodiode (APD) detector module operating in photon-counting mode. Since the APD active area is  $170 \mu\text{m}$  in diameter, its size dictated the type of fiber optic cable that could feed photons to it, to avoid over-filling the detector area. The fiber that was used was a custom multi-mode  $105 \mu\text{m}$  core diameter fiber with a numerical aperture (NA) of 0.22. This fiber size and NA made it the field stop of the receiver system, and defined the full FOV of the system to be  $150 \mu\text{rad}$ . The narrow FOV coupled with the shadow from the secondary mirror of the telescope within our FOV meant that our system would not come into full overlap until about 1.8 km [53]. While the overlap factor will cancel out of the DIAL equation, the overlap limitation will limit the return signal until full overlap is achieved.

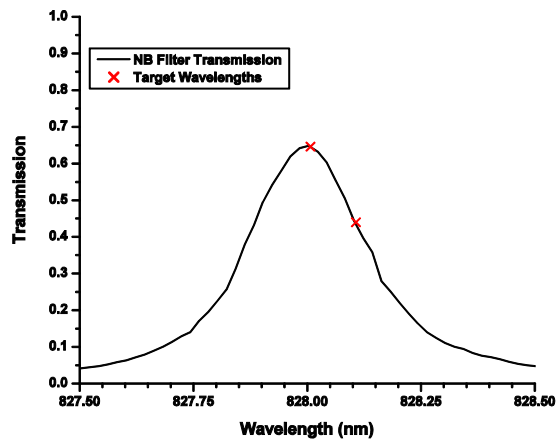


Fig. 7. A plot showing the transmission curve for the narrowband filter, with the DIAL on-line (828.0069 nm) and off-line (828.1069 nm) wavelengths labeled. Data for the transmission were provided courtesy of Barr Associates.

The APD detector (Perkin-Elmer SPCM-AQR-13-FC) is a self-contained single photon counting module requiring only a 5 V input and no external cooling. The output of the detector is a TTL pulse for every detected photon over a range of 400 to 1100 nm. The advantage of using APD's in low-power DIAL experiments is their high peak photon detection efficiency of  $\sim 74\%$  at 700 nm. The other primary detector that would work in this wavelength region is a photomultiplier tube (PMT), but their detection efficiency is much lower, perhaps  $\sim 20\%$  at most. The advantage of PMT's is that they typically have large detector active areas, whereas the APD active area is  $170 \mu\text{m}$  in diameter, making alignment critical. A GRIN lens is glued to the interior of the APD housing that projects an image of the fiber magnified by a factor of 1.4 onto the detector area. The maximum count rate of the APD is nominally 15 Mc/s, with a dead time of 50 ns between pulses. If the count rate exceeds about 1 Mc/s, photons will go undetected because the APD does not have adequate time to reset between detections, and therefore a correction factor must be applied to the output. APD's in photon counting mode are amazingly sensitive to all sources of light, and therefore had to be isolated from all light sources to allow for accurate signal counts.

### 3.3 Data acquisition and control

The TTL logic pulses that originate from the APD detector are then counted and binned in time by a multi-channel scalar (MCS, ASRC Aerospace AMCS-USB), which makes range resolution possible. The fastest rate at which the MCS could be triggered, and therefore the fastest rate at which we could pulse the laser, was 20 kHz.

LabVIEW software was used to create the operational code for the water vapor DIAL, and operated in the following manner. The software, operating via GPIB connections, initialized the MCS card and all instruments. It then grabbed the date and time for the purposes of file labeling, and for time-stamping every second (20,000 laser pulses) of data. A custom waveform was selected on the arbitrary waveform generator (AWG) that created the desired pulse, typically a 1  $\mu$ s pulsewidth at a repetition rate of 20 kHz. Pulses of different sizes could be selected based on the desired range resolution and transmitted energy output. The AWG triggered the APD to begin collecting data but the laser pulse was not activated until 5  $\mu$ s later, allowing for a background light measurement to be made. The ECDL PZT voltage was set to zero to initialize it for tuning. The laser was allowed to settle for 5 seconds at the zero PZT voltage and the MCS memory buffer was cleared and readied for data collection. The laser was then tuned to the on-line wavelength and allowed to equilibrate for 5 seconds. A feedback loop using a wavemeter, described in Refs. 54 and 55, tuned the laser wavelength until the on-line wavelength was reached and held it to within  $\pm$  88 MHz (the frequency accuracy of the wavemeter) for the duration of the measurement [54,55]. This wavelength and the reference power were measured. The MCS collected data for one second across 500 bins of 50 ns each. A time stamp, the wavelength and reference power, and these bins were recorded to a data file. This procedure of recording wavelength, reference power, and photon counts was repeated as long as desirable at this wavelength, typically 60 seconds, before the laser was tuned to the off-line wavelength and the procedure was repeated there, typically for 90 seconds. The difference in averaging times helped alleviate the lower transmission of the off-line wavelength through the NB filter. At the end of the off-line measurement period, the PZT voltage is taken to zero before being switched back to the on-line voltage setting to avoid hysteresis in the PZT. This on- and off-line tuning continued as long as was necessary, typically for 3-5 hours per data run, and was completely automated. The LabVIEW code allowed for real-time display of the wavelength for monitoring tuning, the reference power, and the bin counts.

After the data were taken, MATLAB software was used to analyze it. The analysis code scanned the data set and removed data that did not fit within the wavelength stability requirement of  $\pm$ 160 MHz of the chosen wavelength. It then averaged the data spatially, binning the counts according to the resolution defined by the pulse width, or 150 meters for 1  $\mu$ s pulses. After spatial averaging, the software normalized the counts with power and subtracted the background measurement from the overall data on a second-by-second basis to increase accuracy. Temporal averaging was typically performed over an hour of data to collect enough signal without allowing the atmosphere to change drastically. The long averaging times required by low-power systems have been shown to lead to biases in data [7], and indeed, our results showed strong disagreements on nights when the atmosphere was changing rapidly, such as on windy nights or when a storm system was entering the area. Therefore, measurements were limited to calm nights with stable atmospheric conditions for this initial study. The averaged and background subtracted counts were then used with absorption cross section values generated from radiosonde temperature and pressure measurements to calculate water vapor profiles using the DIAL equation.

### 3.4 System layout

The ECDL output was circularized by an anamorphic prism pair before passing through two Faraday isolators to prevent optical feedback from affecting the performance of the ECDL or damaging the diode laser. After the isolators, the light is incident on a half-wave plate and polarizing beam splitter (PBS) combination, which was used to launch part of the ECDL beam into an optical fiber for monitoring the ECDL wavelength on a wavemeter with an accuracy in frequency of  $\pm 88$  MHz, while the second polarization output of the PBS was free-space coupled into the first tapered amplifier by using two irises for alignment. The first TA output was collimated and sent through a Faraday isolator preventing damage to the tapered amplifier from optical feedback and second half-wave plate and PBS for monitoring. One polarization output of the second PBS was launched into an optical fiber for monitoring the output of the first tapered amplifier on an OSA with a resolution of 0.1 nm. The second polarization output of this PBS was transmitted through two mirrors, widely-spaced irises, and a collimating lens to seed the second tapered amplifier. The amplifiers needed to be seeded carefully to force them to operate in a single longitudinal mode; otherwise power that would be contained within the output laser linewidth of the TA would be lost to amplified spontaneous emission, decreasing the overall measured power. The output of this TA was similarly sent through an optical isolator and half-wave plate and PBS for monitoring. The transmit light was focused and incident on a mirror that turned the beam vertically onto the vertical breadboard. All mirrors and optics were coated near 830 nm to minimize scattering and raise system efficiency. The transmit beam was sent through an AOM where the first-order diffracted beam was used along with a spatially selective iris to pulse the cw laser beam. The transmit beam was collimated to a diameter of roughly 9 mm after the iris. The transmit beam was passed through a  $\sim 4\%$ -reflective beam splitter before being transmitted. The reflected signal was sent to a reference detector to monitor changes in the transmit power as the transmitter tuned. These fluctuations were normalized out of the final data. The remaining 96% of the light was transmitted into the atmosphere. The DIAL was designed to be bistatic, with the transmit beam being sent around the outside of the telescope, and off of a 45-degree mirror mount epoxied to the top of the receiver telescope's secondary mirror housing. Sending the transmit beam off of the back of the secondary telescope mirror allowed the system to be coaligned at ground level, and took some of the alignment uncertainty out of the bistatic approach. The final system is shown in Fig. 8 and described fully in Obland, 2007a [56].

## 4 SYSTEM CHARACTERIZATION

Many tests and diagnostics were run to verify that the DIAL instrument would be able to meet the stringent requirements for accurate DIAL data. Basic tests were performed that monitored the system transmit power at the transmit mirror and compared it to the reference power being measured to verify that the power fluctuation normalization method was sound. The beam shape of the DIAL system was measured using an imaging camera and was determined to be nearly Gaussian, as expected. Other tests were needed to verify the correct laser wavelength output, the speed and stability of the tuning system, the ability of the transmitter to fine-tune across water vapor absorption lines, and the spectral purity of the transmit beam.

Testing to ensure that the wavelength of the transmit beam after being passed through the AOM was the same as that of the ECDL was performed by measuring both wavelengths and forming their ratio for comparison as the ECDL tuned. Results of these tests show that the wavelength output of the DIAL agrees with the wavelength being measured from the ECDL to within the uncertainty of the commercial wavemeter used in the tests:  $\pm 0.2$  pm.



Fig. 8. A picture of the DIAL instrument in its operational form inside the rooftop room of Cobleigh Hall at Montana State University.

The speed and stability of the extended tuning system that controlled the DIAL on- and off-line tuning was tested in two ways and are described completely in Obland, 2007b [55]. First, the speed and stability of the tuning system was characterized through direct measurement of the laser wavelength as it locked onto the target on- or off-line wavelength. Second, a differential absorption measurement of water vapor contained in a multi-pass gas absorption cell was used to verify that the system was indeed tuning on and off of a water vapor absorption line. These tests demonstrated that the DIAL has the ability to tune on and off of a water vapor absorption line, a frequency jump of 44 GHz, repeatedly and mode-hop-free in under ten seconds. The laser frequency is held stable to within  $\pm 88$  MHz, a necessary requirement for DIAL performance [7]. The frequency stability was limited to  $\pm 88$  MHz due to the accuracy of the wavemeter in use. This performance was shown to be maintainable for tens of seconds to over an hour at each wavelength.

Initial horizontal pulsed absorption measurements were taken by this system on three water vapor absorption lines, 829.022 nm, 831.615 nm, and 831.850 nm, at varying distances using hard targets to maximize the return signal and test the fine tuning ability of the transmitter. Data taken on the 831.615 nm absorption line proved to be too weak to be reliable and so the lidar was coarse-tuned to the slightly stronger 831.850 nm line instead, demonstrating the powerful flexibility of a system able to tune to several absorption lines. Pulses 500 ns wide, leading to 75-m-long rangebins and average pulse energies of 50 nJ per pulse, were transmitted at a repetition rate of 500 Hz. Signal averaging of typically 100 seconds was used to increase the return signal and smooth out short-timescale variations. An average of the off-line data was taken and used to normalize the entire data spectrum.

Data sets from two water vapor lines compared to HiTRAN predictions illustrating the system tunability are shown in Figs. 9 and 10. Figure 9 shows tuning data taken across the 829.022 nm water vapor line at pathlengths of 1.71 km and 0.35 km. Figure 10 shows tuning data taken across the 831.850 nm water vapor absorption line at pathlengths of 1.67 km and 0.35 km. The varying pathlengths can be thought of as equivalent to the system response to varying relative humidities, as the absorption lines would become more or less pronounced depending on the water vapor density present in the atmosphere. The temperature and relative humidity measurements were made by a weather station located a few meters above the lidar and were averaged over the typically 1 hour or more needed to take all of the data points. Taken together, these figures from the horizontal pulsed measurements show the capability of the ECDL/TA transmitter to selectively probe different water vapor absorption lines depending on current atmospheric conditions.

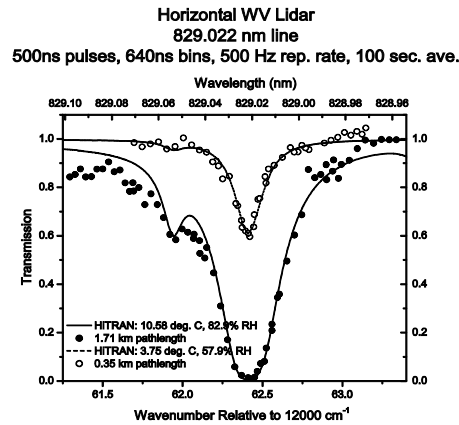


Fig. 9. A plot of the relative transmission through the atmosphere as a function of wavelength near 829.022 nm. The open (closed) circles represent measurements made for a 0.35 km (1.71 km) path length. The solid and dashed lines are theoretical calculations using HiTRAN-PC with the measured temperature, humidity, and path length.

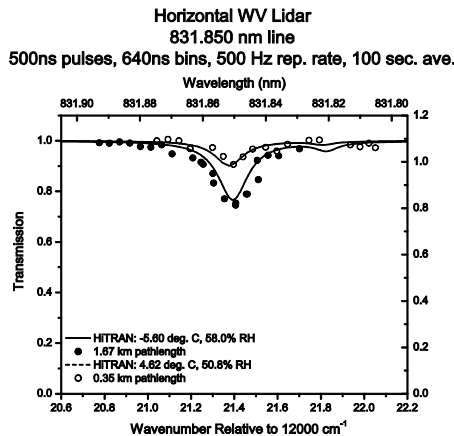


Fig. 10. A plot of the relative transmission through the atmosphere as a function of wavelength near 831.850 nm. The open (closed) circles represent measurements made for a 0.35 km (1.67 km) path length. The solid and dashed lines are theoretical calculations using HiTRAN-PC with the measured temperature, humidity, and path length.

Spectral purity is defined as the fraction of laser power within the water-vapor absorption line width with respect to the entire output pulse power of the laser. It is a critical parameter for accurate DIAL measurements because the assumption is made in the DIAL equation that the laser is nearly monochromatic, and therefore all the laser light is absorbed uniformly by an absorption line. If, however, the laser power is spread across a larger spectrum, the laser power will be absorbed differently at each wavelength, and the functional dependence of the laser output power with wavelength must be well known to invert the DIAL equation.

Other techniques for measuring spectral purity have been used [9]. To measure the spectral purity of the MSU DIAL we measured the power of the laser transmitter as a function of wavelength within the bandwidth of the receiver using a calibrated OSA. We integrated the

power spectrum across the linewidth of the laser and compared this value to the integrated total power across the receiver bandwidth. The ratio of these two values provides the spectral purity. As previously stated, the linewidth of the laser is known to be <200 kHz [50]. The knowledge of the linewidth coupled with the frequency stability and accuracy shows that the laser linewidth is completely contained within the water vapor absorption linewidth. Tests were run to determine that the spectral purity was not affected by the use of the AOM, or the type or length of optical fiber in the receiver. The spectral purity of the transmitter was measured to be >0.995 at the on-line wavelength and >0.992 at the off-line wavelength. Note that the spectral purity for the off-line wavelength does not meet the spectral purity requirements stated in the literature [7], but this should not matter because the off-line wavelength is far removed from any water vapor absorption lines, and therefore the uniform absorption assumption still holds. These tests show that the spectral purity of the DIAL is adequate for accurate water vapor retrievals.

The spectral requirements for DIAL measurements with an error due to individual laser properties of <3% are stringent [7], yet were still met or exceeded by the final MSU DIAL instrument. These requirements are compared to the current MSU DIAL system parameters in Table 2. Note that the requirement for on-/off-line switching time is only a guideline, as longer times can lead to biases in atmospheric retrievals [7].

Table 2. DIAL system properties.

| Parameter                                 | Measured Value                 | Requirement (at 830 nm) |
|---|--------------------------------|-------------------------|
| <b>Transmitter</b>                        |                                |                         |
| On-/Off-line Wavelength (nm, vacuum)      | 828.187/828.287                |                         |
| Repetition Rate (kHz)                     | 20                             |                         |
| Pulse Width ( $\mu$ s)                    | 1.0                            |                         |
| Pulse Energy ( $\mu$ J)                   | ~0.25                          |                         |
| Linewidth (FWHM; MHz)                     | <0.300                         | <298                    |
| Frequency Stability (MHz)                 | +/-88                          | +/-160                  |
| Spectral Purity                           | 0.995                          | >0.995                  |
| On-/Off-line Switching Time               | ~ 60-90 sec.                   | <~1 ms                  |
| <b>Optical Receiver</b>                   |                                |                         |
| Telescope Diameter (cm)                   | 28                             |                         |
| Far-field Full Field of View ( $\mu$ rad) | 150                            |                         |
| Filter Bandwidth (pm)                     | ~250                           |                         |
| <b>Detection Electronics</b>              |                                |                         |
|   | APD with Geiger-mode detection |                         |

## 5 MEASUREMENTS

An example of on- and off-line background-subtracted counts averaged over time is shown in Fig. 11, with the y-axis displaying total counts and the x-axis showing altitude in meters above the laser instrument. Raw counts are also shown for comparison. The bins located below zero altitude are used for background determination and subtraction. The flash of the laser pulse is seen at zero altitude and lasts for approximately three range bins due to the poorly-shielded detector box allowing stray reflected light to illuminate the detector after the initial flash and from strong near-field atmospheric returns due to misalignment of the transmitter and receiver. The initial flash of the laser is so weak that a correction factor for the APD counts was not needed, as the APD was not near saturation levels. The averaged counts such as these are used in the DIAL equation to calculate water vapor density bin-by-bin.

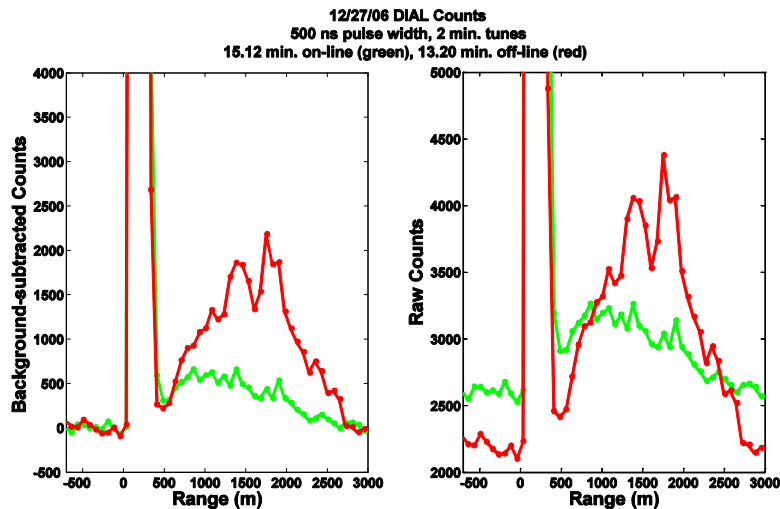


Fig. 11. A comparison of background-subtracted and raw return photon counts for the DIAL instrument for a sample measurement with the y-axis displaying total counts and the x-axis showing altitude in meters above the laser instrument. The bins below zero meters in range are used for background determination and subtraction. The flash of the laser pulse is seen at zero altitude. The averaged counts such as these are used in the DIAL equation to calculate water vapor density bin-by-bin.

To verify that the water vapor DIAL was measuring the accurate amount of water vapor, radiosondes were launched with each DIAL data run to give an *in situ* measurement of temperature and relative humidity, which were then converted to water vapor number density for direct comparison with the DIAL measurements. Initial water vapor profiles were taken on many nights and their agreement with co-located radiosondes is altitude dependent: reasonable agreement was found at altitudes greater than about 800 meters while the two measurements did not agree below 800 meters. The data were typically averaged over about 1 hour with pulse widths of 1  $\mu$ s. Dry winter conditions at the time the measurements were taken probably put the instrument near its water vapor detection limit, but signals should improve as water vapor increases during spring and summer measurements. Data above about 800 meters showed reasonable agreement with the co-located radiosonde with differences ranging between about 5% and 60%, but within the calculated error limits. Below 800 meters, the data do not agree within the error limits, with the measurements being separated by almost 300% in the lowest range bin. At almost all ranges, the DIAL-measured water vapor is biased low compared to the radiosonde. The major reason for the lack of agreement at low altitudes has subsequently been shown, since the submission of this manuscript, to be that the center wavelength, and therefore transmission characteristics, of the very narrow-band filter will change for photons that pass through the filter at a high angle of incidence, such as those from low altitudes [57]. A correction factor is needed to account for this change in filter transmission, and when implemented, leads to improved measurements [57]. Possible causes for the overall bias include inadequate shielding of the detector from spurious background light leakage that is unaccounted for in the background removal algorithm, which has the effect in the DIAL equation of reducing the amount of water vapor, the misalignment of the transmitter with the receiver, and slow switching times between on- and off-line wavelengths.

With improvements to the system to reduce spurious light contamination, increase alignment of the receiver with the transmitted beam, correct for the very narrow-band filter transmission [57] and Doppler-broadened Rayleigh backscatter effect [6, 58], and decrease the time between on- and off-line measurements, this low-power DIAL system has shown potential to achieve meaningful water vapor profiles up to at least 2 km and potentially more

with longer temporal and spatial averaging and increased transmit power [57, 59]. The ability to produce such results is a major step towards proving the viability of this system for field deployments, and should only improve with future versions of the instrument.

## 6 CONCLUSION

A compact, low-power differential absorption lidar (DIAL) using a widely tunable diode laser was built, tested, and used to produce profiles of atmospheric water vapor up to an altitude of 2 km above ground level. The transmitter for the DIAL used an external cavity diode laser (ECDL) that was built through the expertise of the laser source development group at Montana State University (MSU) coupled with two cascaded commercial tapered amplifiers (TA). The ECDL has the capability of tuning across a 17 nm spectrum near 830 nm, giving it access to numerous water vapor absorption lines.

The tunability of the transmitter was first shown through horizontally pointing lidar experiments in which the laser was tuned across water vapor absorption lines at wavelengths of 829.022 nm, 831.615 nm, and 831.850 nm. The scans were compared and were in agreement to within a few percent of the absorption values given by HiTRAN-PC atmospheric modeling software.

This transmitter was then coupled into a vertically-pointing DIAL instrument. The DIAL used an acousto-optic modulator (AOM) to pulse the cw beam from the transmitter. The receiver made use of a commercial Schmidt-Cassegrain telescope with a diameter of 28 cm, an extremely narrow band (NB) filter with a band pass of  $\sim 250$  pm, and a fiber-coupled, photon counting avalanche photodiode (APD) detector, and had a narrow, 150  $\mu$ rad field of view (FOV). Both coaxial and bistatic configurations were attempted, with the bistatic approach producing successful results. The DIAL system was almost completely autonomously controlled using LabVIEW software and a novel tuning system that quickly tuned the ECDL between the on-line vacuum wavelength of 828.187 nm and off-line vacuum wavelength of 828.287 nm. The tuning mechanism was extensively tested, showing that the laser wavelength could be held stable to within  $\pm 88$  MHz, well within the requirement of  $\pm 160$  MHz for accurate water vapor profiles. The spectral purity was measured to be  $>0.995$ , within allowable tolerances.

Pulses with widths of 1.0  $\mu$ s and energies of  $\sim 0.25$   $\mu$ J, at a repetition rate of 20 kHz, were used to probe the lower troposphere up to 2 km, resulting in water vapor profiles that were compared to co-located radiosonde measurements. The initial DIAL measurements agreed to within 5-60% with the radiosonde 800 meters above ground altitude. Below 800 meters, the measurements are biased low due to a number of systematic issues that are being corrected with modifications to the instrument. Making these changes to the DIAL would create a second-generation instrument capable of accurate nighttime and potentially daytime water vapor profiles up to at least 2 km.

This DIAL instrument has demonstrated that low-power DIAL instruments using widely tunable diode laser transmitters, which can be designed at multiple wavelengths, can achieve useful water vapor profiles. The system is robust, can be repaired quickly and relatively easily, compact, and can be made eye-safe, all necessary requirements for an autonomous field instrument. It is hoped that this DIAL will lead to the development of next-generation, widely tunable DIAL instruments that in the future may be acceptable candidates for use in multi-point lidar networks to study water vapor flux profiles.

## Acknowledgments

This work was supported by NASA grant number NNX06AD11G and the NASA Graduate Student Research Program (GSRP), and partially supported by NASA EPSCoR grant number NNX08AT69A. At the time this research was performed, Michael Obland was a graduate

student at Montana State University. He has since become a research scientist at NASA Langley Research Center, initially as a NASA Postdoctoral Fellow, administered by Oak Ridge Associated Universities through a contract with NASA.

## References

- [1] J. E. Harries, "Atmospheric radiation and atmospheric humidity," *Quart. J. Roy. Meteor. Soc.* **123**, 2173-2186 (1997) [doi:10.1256/smsqj.54401].
- [2] Y. Han and E. R. Westwater, "Remote sensing of tropospheric water vapor and cloud liquid water by integrated ground-based sensors," *J. Atmos. Ocean. Technol.* **12**, 1050-1059 (1995) [doi:10.1175/1520-0426(1995)012<1050:RSOTWV>2.0.CO;2].
- [3] D. D. Turner, W. F. Feltz, and R. A. Ferrare, "Continuous water vapor profiles from operational active and passive remote sensors," *Bull. Am. Meteorol. Soc.* **81**, 1301-1317 (2000) [doi:10.1175/1520-0426(1995)012<1050:RSOTWV>2.0.CO;2].
- [4] T. M. Weckwerth, V. Wulfmeyer, R. M. Wakimoto, R. M. Hardesty, J. W. Wilson, and R. M. Banta, "NCAR-NOAA lower-tropospheric water vapor workshop," *Bull. Am. Meteorol. Soc.* **80**, 2339-2357 (1999) [doi:10.1175/1520-0477(1999)080<2339:NNLTWV>2.0.CO;2].
- [5] J. A. R. Rall, "Differential absorption lidar measurements of atmospheric water vapor using a pseudonoise code modulated AlGaAs laser," NASA Technical Memorandum **104610**, NASA Center for AeroSpace Information, Linthicum Heights, MD (1994).
- [6] J. E. M. Goldsmith, F. H. Blair, S. E. Bisson, and D. D. Turner, "Turn-key Raman lidar for profiling atmospheric water vapor, clouds, and aerosols," *Appl. Opt.* **37**, 4979-4990 (1998) [doi:10.1364/AO.37.004979].
- [7] J. Bosenberg, "Ground-based differential absorption lidar for water-vapor and temperature profiling: methodology," *Appl. Opt.* **37**, 3845-3860 (1998) [doi:10.1364/AO.37.003845].
- [8] V. Wulfmeyer, "Ground-based differential absorption lidar for water-vapor and temperature profiling: development and specifications of a high-performance laser transmitter," *Appl. Opt.* **37**, 3804-3860 (1998) [doi:10.1364/AO.37.003804].
- [9] V. Wulfmeyer and J. Bösenberg, "Ground-based differential absorption lidar for water-vapor profiling: assessment of accuracy, resolution, and meteorological applications," *Appl. Opt.* **37**, 3825-3844 (1998) [doi:10.1364/AO.37.003825].
- [10] V. Wulfmeyer, "Investigation of turbulent processes in the lower troposphere with water vapor DIAL and radar-RASS," *J. Atmos. Sci.* **56**, 1055-1076 (1999) [doi:10.1175/1520-0469(1999)056<1055:IOTPIT>2.0.CO;2].
- [11] V. Wulfmeyer and C. Walther, "Future performance of ground-based and airborne water vapor differential absorption lidar: I. Overview and theory," *Appl. Opt.* **40**, 5304-5320 (2001) [doi:10.1364/AO.40.005304].
- [12] D. D. Turner, R. A. Ferrare, L. A. Heilman Brasseur, W. F. Feltz, and T. P. Tooman, "Automated retrievals of water vapor and aerosol profiles from an operational Raman lidar," *J. Atmos. Ocean. Technol.* **19**, 37-50 (2002) [doi:10.1175/1520-0426(2002)019<0037:AROWVA>2.0.CO;2].
- [13] G. Ehret, C. Kiemle, R. Renger, and G. Simmet, "Airborne remote sensing of tropospheric water vapor with a near-infrared differential absorption lidar system," *Appl. Opt.* **32**, 4534-4551 (1993) [doi:10.1364/AO.32.004534].
- [14] S. Ismail, E. V. Browell, R. A. Ferrare, S. A. Kooi, M. B. Clayton, V. G. Brackett, and P. B. Russell, "LASE measurements of aerosol and water vapor profiles during TARFOX," *J. Geophys. Res.* **105**, 9903-9916 (2000) [doi:10.1029/1999JD901198].

- [15] G. Ehret, A. Fix, V. Weiss, G. Poberaj, and T. Baumert, "Diode-laser-seeded optical parametric oscillator for airborne water vapor DIAL application in the upper troposphere and lower stratosphere," *Appl. Phys. B* **67**, 427–431 (1998) [doi:10.1007/s003400050526].
- [16] E. V. Browell, S. Ismail, and W. B. Grant, "Differential absorption lidar (DIAL) measurements from air and space," *Appl. Phys. B* **67**, 399-410 (1998) [doi:10.1007/s003400050523].
- [17] D. Bruneau, P. Quaglia, C. Flamant, M. Meissonnier, and J. Pelon, "Airborne lidar LEANDRE II for water-vapor profiling in the troposphere. I. system description," *Appl. Opt.* **40**, 3450-3461 (2001) [doi:10.1364/AO.40.003450].
- [18] D. Bruneau, P. Quaglia, C. Flamant, and J. Pelon, "Airborne lidar LEANDRE II for water-vapor profiling in the troposphere. II. first results," *Appl. Opt.* **40**, 3462-3475 (2001) [doi:10.1364/AO.40.003462].
- [19] C. Kiemle, W. A. Brewer, G. Ehret, R. M. Hardesty, A. Fix, C. Senff, M. Wirth, G. Poberaj, and M. A. LeMone, "Latent heat flux profiles from collocated airborne water vapor and wind lidars during IHOP 2002," *J. Atmos. Ocean. Technol.* **24**, 627-639 (2007) [doi:10.1175/JTECH1997.1].
- [20] C. Kiemle, M. Wirth, A. Fix, G. Ehret, U. Schumann, T. Gardiner, C. Schiller, N. Sitnikov, and G. Stiller, "First airborne water vapor lidar measurements in the tropical upper troposphere and mid-latitudes lower stratosphere: accuracy evaluation and intercomparisons with other instruments," *Atmos. Chem. Phys.* **8**, 5245-5261 (2008)
- [21] J. D. Spinhirne, "Micro pulse lidar," *IEEE Trans. Geosci. Remote Sens.* **31**, 48-55 (1993) [doi:10.1109/36.210443].
- [22] J. A. R. Rall and J. B. Abshire, "Antarctic miniature lidar," *IEEE Int. Geosci. Rem. Sens. Symp.*, 1538-1540 (1996).
- [23] J. A. Shaw, J. J. Bates, W. L. Eberhard, R. J. Alvarez II, S. P. Sandberg, and L. Larrabee Strow, "Atmospheric measurements with unattended FTIR and Lidar," in *Technical Digest, Topical Meeting on Optical Remote Sensing of the Atmosphere*, pp. 77-79, Opt. Soc. Am., Washington, D.C. (2001).
- [24] J. R. Campbell, D. L. Hlavka, E. J. Dutton, C. J. Flynn, D. D. Turner, J. D. Spinhirne, V. S. Scott III, and I. H. Hwang, "Full-time, eye-safe cloud and aerosol lidar observation at atmospheric radiation measurement program sites: Instruments and data processing," *J. Atmos. Ocean. Technol.* **19**, 431-442 (2002) [doi:10.1175/1520-0426(2002)019<0431:FTESCA>2.0.CO;2].
- [25] J. M. Intrieri, M. D. Shupe, T. Uttal, and B. J. McCarty, "An annual cycle of Arctic cloud characteristics observed by radar and lidar at SHEBA," *J. Geophys. Res.* **107** (C10), SHE5-1-15 (2002) [doi:10.1029/2000JC000423].
- [26] W. B. Grant, "Differential absorption and Raman lidar for water vapor profile measurements: a review," *Opt. Eng.* **30**, 40-45 (1991) [doi:10.1117/12.55772].
- [27] R. M. Measures, *Laser Remote Sensing: Fundamentals and Applications*, Krieger, Malabar, FL (1992).
- [28] V. A. Kovalev and W. E. Eichinger, *Elastic Lidar: Theory Practice, and Analysis Methods*, Wiley-Interscience, Hoboken, NJ (2004) [doi:10.1002/0471643173].
- [29] J. A. Reagan, T. W. Cooley, and J. A. Shaw, "Prospects for an economical, eye-safe water vapor LIDAR," *IEEE Int. Geosci. Rem. Sens. Symp.*, 872-874 (1993).
- [30] J. A. Reagan, H. Liu, and J. F. McCalmont, "Laser diode based new generation lidars," *IEEE Int. Geosci. Rem. Sens. Symp.*, 1535-1537 (1996).
- [31] C. R. Prasad, V. A. Fromzel, J. S. Smucz, I. H. Hwang, and W. E. Hasselbrack, "A diode-pumped Cf:LiSAF laser for UAV-based water vapor differential absorption lidar (DIAL)," *IEEE Int. Geosci. Rem. Sens. Symp.*, 1465-1467 (2000).

- [32] L. M. Little and G. C. Papen, "Fiber-based lidar for atmospheric water-vapor measurements," *Appl. Opt.* **40**, 3417-3427 (2001) [doi:10.1364/AO.40.003417].
- [33] S. Penchev, S. Naboko, V. Naboko, V. Pencheva, T. Donchev, L. Pavlov, and P. Simeonov, "DIAL monitoring of atmospheric climate-determining gases employing high-power pulsed laser diodes," *Proc. SPIE* **5226**, 290-294 (2003) [doi:10.1117/12.519502].
- [34] J. L. Machol, T. Ayers, K. T. Schwenz, K. W. Koenig, R. M. Hardesty, C. J. Senff, M. A. Krainak, J. B. Abshire, H. E. Bravo, and S. P. Sandberg, "Preliminary measurements with an automated compact differential absorption lidar for the profiling of water vapor," *Appl. Opt.* **43**, 3110-3121 (2004) [doi:10.1364/AO.43.003110].
- [35] C. Oh, C. R. Prasad, V. Fromzel, I. H. Hwang, J. A. Reagan, H. Fang, and M. Rubio, "Water vapor micro pulse differential absorption lidar," *Proc. SPIE* **3703**, 177-186 (1999) [doi:10.1117/12.351342].
- [36] C. E. Wieman and L. Hollberg, "Using diode lasers for atomic physics," *Rev. Sci. Instrum.* **62**, 1-20, (1991) [doi:10.1063/1.1142305].
- [37] L. S. Meng, K. S. Repasky, P. A. Roos, and J. L. Carlsten, "Widely tunable continuous-wave Raman laser in diatomic hydrogen pumped by an external-cavity diode laser," *Opt. Lett.* **25**, 472-474 (2000) [doi:10.1364/OL.25.000472].
- [38] K. S. Repasky, P. A. Roos, L. S. Meng, and J. L. Carlsten, "Amplified output of a frequency chirped diode source via injection locking," *Opt. Eng.* **40**, 2505-2509 (2001) [doi:10.1117/1.1412620].
- [39] L. S. Rothman, A. Barbe, D. C. Benner, L. R. Brown, C. Camy-Peyret, M. R. Carleer, K. Chance, C. Clerbaux, V. Dana, V. M. Devi, A. Fayt, J.-M. Flaud, R. R. Gamache, A. Goldman, D. Jacquemart, K. W. Jucks, W. J. Lafferty, J.-Y. Mandin, S. T. Massie, V. Nemtchinov, D. A. Newnham, A. Perrin, C. P. Rinsland, J. Schroeder, K. M. Smith, M. A. H. Smith, K. Tang, R. A. Toth, J. Vander Auwera, P. Varanasi, and K. Yoshino, "The HITRAN molecular spectroscopic database: edition of 2000 including updates through 2001," *J. Quant. Spectrosc. Radiat. Trans.* **82**, 5-44 (2003) [doi:10.1016/S0022-4073(03)00146-8].
- [40] R. M. Schotland, "Some observations of the vertical profile of water vapor by means of a ground based optical radar," *Proc. 4th Symp. Rem. Sens. Environ.*, 273-283, Univ. Michigan, Ann Arbor, MI (1966).
- [41] E. V. Browell, S. Ismail, and B. E. Grossmann, "Temperature sensitivity of differential absorption lidar measurements of water vapor in the 720-nm region," *Appl. Opt.* **30**, 1517-1524 (1991) [doi:10.1364/AO.30.001517].
- [42] P. F. Ambrico, A. Amodeo, P. di Girolamo, and N. Spinelli, "Sensitivity analysis of differential absorption lidar measurements in the mid-infrared region," *Appl. Opt.* **39**, 6847-6865 (2000) [doi:10.1364/AO.39.006847].
- [43] E. E. Remsberg and L. L. Gordley, "Analysis of differential absorption lidar from the Space Shuttle," *Appl. Opt.* **17**, 624-630 (1978) [doi:10.1364/AO.17.000624].
- [44] V. Wulfmeyer, "DIAL – Messungen von vertikalen Wasserdampfverteilungen-ein Lasersystem für Wasserdampf- und Temperaturmessungen in der Troposphäre," PhD. Dissertation, Max-Planck-Institut für Meteorologie, Hamburg, Germany (1995).
- [45] V. Wulfmeyer and C. Walther, "Future performance of ground-based and airborne water-vapor differential absorption lidar. II. simulations of the precision of a near-infrared, high-power system," *Appl. Opt.* **40**, 5321-5336 (2001) [doi:10.1364/AO.40.005321].
- [46] J. A. Shaw, <http://www.coe.montana.edu/ee/weather/> (2008).
- [47] M. G. Littman and H. J. Metcalf, "Spectrally narrow pulsed dye laser without beam expander," *Appl. Opt.* **17**, 2224-2227 (1978) [doi:10.1364/AO.17.002224].

- [48] P. McNicholl and H. J. Metcalf, "Synchronous cavity mode and feedback wavelength scanning in dye laser oscillators with gratings," *Appl. Opt.* **24**, 2757-2761 (1985) [doi:10.1364/AO.24.002757].
- [49] M. de Labacherie and G. Passadat, "Mode-hop suppression of Littrow grating-tuned lasers," *Appl. Opt.* **32**, 269-274 (1993) [doi:10.1364/AO.32.000269].
- [50] K. S. Repasky, G. W. Switzer, and J. L. Carlsten, "Design and performance of a frequency chirped external cavity diode laser," *Rev. Scientific Instr.* **73**, 3154-3159 (2002) [doi:10.1063/1.1499541].
- [51] New Focus Product Guide, **15**, 20-39, San Jose, CA (2007).
- [52] G. W. Switzer "Semiconductor laser transmitter for water vapor lidar on Mars," Ph.D. Thesis, Montana State University, Bozeman, MT (1999).
- [53] K. Stelmaszczyk, M. Dell'Aglio, S. Chudzyński, T. Stacewicz, and L. Wöste, "Analytical function for lidar geometrical compression form-factor calculations," *Appl. Opt.*, **44**, 1323-1331 (2005) [doi: 10.1364/AO.44.001323].
- [54] K. S. Repasky, A. R. Nehrir, J. T. Hawthorne, G. W. Switzer, and J. L. Carlsten, "Extending the continuous tuning range of an external cavity diode laser," *Appl. Opt.* **45**, 9013-9020 (2006) [doi:10.1364/AO.45.009013].
- [55] M. D. Obland, A. R. Nehrir, K. S. Repasky, J. L. Carlsten, and J. A. Shaw, "Application of extended tuning range for external cavity diode lasers to water vapor differential absorption measurements," *Opt. Eng.* **46**, 084301 (2007b) [doi:10.1117/1.2771654].
- [56] M. D. Obland, "Water vapor profiling using a widely tunable amplified diode laser differential absorption lidar (DIAL)," Ph.D. Dissertation, Montana State University, Bozeman, MT, <http://etd.lib.montana.edu/etd/2007/obland/OblandM0507.pdf> (2007a).
- [57] A. R. Nehrir, K. S. Repasky, J. L. Carlsten, M. D. Obland, and J. A. Shaw, "Water vapor profiling using a widely tunable, amplified diode-laser-based Differential Absorption Lidar (DIAL)," *J. Atmos. Ocean. Technol.* **26**, 4, 733-745 (2009) [doi: 10.1175/2008JTECHA1201.1].
- [58] A. Ansmann, "Errors in ground-based water-vapor DIAL measurements due to Doppler-broadened Rayleigh backscattering," *Appl. Opt.* **24**, 3476-3480 (1985) [doi:10.1364/AO.24.003476].
- [59] A. R. Nehrir, K. S. Repasky, and J. L. Carlsten, "Diode laser based micro-pulse differential absorption lidar (DIAL) for water vapor profiling in the lower troposphere," manuscript in preparation (2010).

**Michael D. Obland** received his bachelor degrees in physics and mathematics from the University of Montana in 2000 and his MS and PhD in physics from Montana State University in 2001 and 2007, respectively, under support from a NASA Graduate Student Researchers Program (GSRP) fellowship through Goddard Space Flight Center. He is now a research scientist working with the airborne High Spectral Resolution Lidar group at NASA Langley Research Center. His research interests include lidar and satellite remote sensing, specifically measuring atmospheric aerosols.

**Amin R. Nehrir** received his BS and MS degrees in Electrical Engineering from Montana State University in 2006 and 2008 respectively. He is currently a Doctoral candidate in the Electrical Engineering department at Montana State University under support from a NASA Graduate Student Researchers Program (GSRP) fellowship through Langley Research Center. His research interests include laser source development, ground based remote sensing and direct detection measurements of atmospheric trace gasses, specifically differential absorption lidar measurements of atmospheric water vapor and carbon dioxide. He is also working on

the development of a photonic band gap sub-surface fiber optic sensor for monitoring CO<sub>2</sub> concentrations above geological CO<sub>2</sub> sequestration sites.

**Kevin S. Repasky** received the B.S.Eng. degree in mechanical engineering from Youngstown State University in 1988 and his M.S. and Ph.D. degrees in physics from Montana State University in 1992 and 1996 respectively. Currently he is an Assistant Professor in the Electrical Engineering Department at Montana State University. His research interests include laser design and development, nonlinear optics, optical remote sensing, and optical communications.

**John L. Carlsten** holds the B.S. degree in Physics from the University of Minnesota (1969) and the M.S. degree and Ph.D. degree in Physics from Harvard University (1974). Currently he holds the position of Regents Professor of Physics at Montana State University. Previously he has held positions at the University of Colorado (1974-1979) and the Los Alamos National Laboratory (1979-1984). His current areas of research involve the study of the quantum optics and nonlinear optics of the diode pumped cw Raman laser, for which he holds a patent along with Professor Kevin Repasky and Dr. Jason Brasseur. He also collaborates with Professors Repasky and Shaw on LIDAR applications to water vapor DIAL, bee detection and carbon dioxide monitoring. Professor Carlsten is a Fellow in the American Physical Society and is a Fellow in the Optical Society of America.

**Joseph A. Shaw** received his B.S. degree in electrical engineering from the University of Alaska - Fairbanks in 1987, M.S. degree in electrical engineering from the University of Utah in 1989, and M.S. and Ph.D. in Optical Sciences from the University of Arizona in 1994 and 1996, respectively. He worked at the National Oceanic and Atmospheric Administration (NOAA) in Boulder, Colorado from 1989 to 2001 on infrared spectro-radiometers and laser sensors for studying the Earth's atmosphere and oceans. Since 2001 he has been on the faculty of Montana State University in Bozeman, Montana where he is currently Professor of Electrical and Computer Engineering. His present research is on polarimetry, radiometry, and laser remote sensing of the natural environment. Dr. Shaw is a Fellow of both SPIE and the Optical Society of America (OSA).